Distortions of $[Sb_2Cl_{10}]^{4-}$ Bioctahedra and Phase Transitions in the Chloroantimonate(III) $(C_3H_5NH_3)_2[SbCl_5] \cdot (C_3H_5NH_3)Cl$

Bartosz Zarychta, Maciej Bujak, and Jacek Zaleski

Institute of Chemistry, University of Opole, Oleska 48, 45-052 Opole, Poland

Reprint requests to Prof. J. Zaleski. Fax: (+48)-77-4410741. E-mail: zaleski@uni.opole.pl

Z. Naturforsch. **2007**, *62b*, 44 – 50; received July 4, 2006

Bis(allylammonium)pentachloroantimonate(III) – allylammonium chloride, $(C_3H_5NH_3)_2[SbCl_5] \cdot (C_3H_5NH_3)Cl$, belongs to the chloroantimonate(III) organic-inorganic salts family. The DSC studies of this compound showed two anomalies at 181 K and at 223 K. Both are associated with phase transitions, which mainly occur due to ordering-disordering processes of the organic cations. Between 181 and 223 K the structure is incommensurate. The crystal structure was determined at 298 and 86 K. At both temperatures the crystal structure consists of $(C_3H_5NH_3)^+$ cations, anionic distorted $[Sb_2Cl_{10}]^{4-}$ units and isolated Cl^- ions. In the room-temperature phase two out of three, and in the low-temperature phase two out of six allylammonium cations were found to be disordered. The deformations of the $[Sb_2Cl_{10}]^{4-}$ moieties in both phases are discussed and explained by the deviation of the Sb^{III} 5*s* electron lone pair from its spherical symmetry and the influence of N–H···Cl hydrogen bonds, which join together the organic and inorganic sublattices.

Key words: Chloroantimonates(III), Phase Transitions, Crystal Structure, Octahedral Distortions, Hydrogen Bonding

Introduction

Halogenoantimonates(III) and halogenobismuthates(III) with organic cations defined by the general formula $R_aM_bX_{3b+a}$ (where *R* is an organic cation; *M* is Sb^{III} or/and Bi^{III} and *X* is Cl, Br or/and I) are an interesting group of compounds due to their ferroelectric properties [1 – 5]. The polarity of these crystals is associated with phase transitions, which are mainly caused by the changes in rotational motions of the organic cations [2, 6]. These phenomena are especially manifested in the structures containing relatively small methyl-, dimethyl-, trimethyl- and tetramethylammonium cations [2, 7 – 10].

Halogenoantimonates(III) and halogenobismuthates(III) are considered as mixed organic-inorganic materials. Their inorganic sublattices are composed of deformed polyhedra – octahedra or square pyramids – which occur isolated or connected with each other by corners, edges or faces and as a consequence form various structural units [*e. g.* 11, 12]. The organic cations are placed in voids of the anionic sublattice. They are usually connected to the inorganic part of the structure by extended and complex N(C)–H···Cl hydrogen bonding and/or N···Cl electrostatic interactions.

This paper is a part of our larger project devoted to the synthesis, structures, phase transitions and molecular motions in halogenoantimonates(III) and halogenobismuthates(III) with organic cations. We have recently reported the structure and properties of tris(allylammonium) hexachlorobismuthate(III), $(C_3H_5NH_3)_3[BiCl_6]$ [13]. This compound was obtained in a reaction of allylamine and basic bismuth(III) carbonate in an aqueous solution of hydrochloric acid. Its structure is composed of isolated, distorted $[BiCl_6]^{3-}$ octahedra and allylammonium cations. We have found in this salt three phase transitions at 152, 191 and 299 K. The mechanism of the high-temperature phase transition is related to the ordering with lowering temperature of one cation located at a special position. It has been assumed, on the basis of the X-ray diffraction studies, that the distortions of the $[BiCl_6]^{3-}$ anions are mainly related to N–H···Cl interactions.

In order to obtain further information about the structure and properties of allylammonium halogenoantimonate(III)/halogenobismuthate(III) salts, we report the synthetic, single-crystal X-ray diffraction and differential scanning calorimetry studies of $(C_3H_5NH_3)_2[SbCl_5] \cdot (C_3H_5NH_3)Cl$.

Experimental Section

$(C_3H_5NH_3)_2[SbCl_5] \cdot (C_3H_5NH_3)Cl$ was obtained in the reaction of allylamine (< 99 %) and antimony(III) chloride (> 99 %; both Merck-Schuchardt, Germany) in molar ratios from 1 : 3 to 1 : 10 in aqueous solutions of hydrochloric acid. Single crystals suitable for X-ray diffraction studies were grown by slow evaporation at constant r. t.

The measurements at 298 and 86 K were performed on an Xcalibur CCD diffractometer with graphite monochromated MoK_α ($\lambda = 0.71073$ Å) radiation. The Oxford Cryosystems cooler was used for the measurement at 86 K. The reflections were measured using the ω-scan technique with $\Delta\omega = 0.75°$ and $\Delta t = 20$ s. The structures were solved by the Patterson Method. All data were subjected to Lorentz, polarization and empirical absorption corrections based on symmetry-equivalent reflections [14, 15]. Fourier maps, at both temperatures, revealed a disorder of two crystallographically independent allylammonium cations. All hydrogen atoms were added using standard geometric criteria, then refined using the riding model and constrained to distances of 0.97, 0.93 and 0.90 Å for CH_2, CH and NH_3 groups, respectively. Their displacement parameters were taken with coefficients 1.5 times larger than the respective parameters of the nitrogen and carbon atoms. The Oxford Diffraction software CrysAlis CCD and CrysAlis RED programs were used during the data collection, cell refinement and data reduction processes [14]. The SHELX-97 program [16] was used for structure solution and refinement. The structure drawings were prepared using the SHELXTL program [16]. Crystallographic data (excluding structure factors) at 298 and 86 K, have been deposited at the Cambridge Crystallographic Data Centre as supplementary publication nos. CCDC 612932 and 612933. Copies of the data can be obtained free of charge from The Cambridge Crystallographic Data Centre *via* www.ccdc.cam.ac.uk/data_request/cif.

The DSC analyses, using both single crystal and powder samples, were performed using a Perkin-Elmer DSC Model 7 with a scanning rate of 10 K/min on cooling/heating in the temperature range 140 – 380 K. The TGA measurements on crystalline samples were carried out with a heating rate of 10 K min^{-1} in the temperature range 295 – 555 K on a TGA 2050 TA Instruments apparatus.

Results and Discussion

Phase transitions

The differential scanning calorimetry studies followed by the thermogravimetric analysis showed that the title compound underwent two low temperature phase transitions at *ca.* 181 K and at 223 K (Fig. 1).

On cooling the first phase transition is of second order. In the diffraction pattern we observed satellite reflections up to the first order. No indications of second order satellites were observed. The refined incommensurate q vector was (0.072, −0.417, −0.454). The first calculations showed that at least some of the atoms of the disordered chains could be described by a crenel modulation function [17], which can resolve the disordered positions by separating two near atoms along the additional dimension x4. Modulated structure refinement will be the subject of further studies. Currently we are looking for better samples allowing for a high quality data set necessary for the refinement of the triclinic modulated structure.

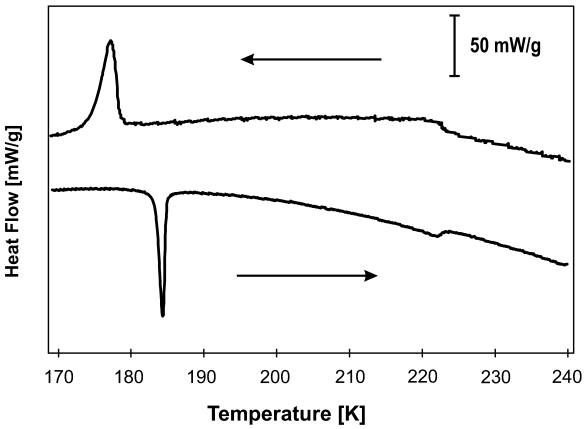

Fig. 1. The DSC diagram of $(C_3H_5NH_3)_2[SbCl_5] \cdot (C_3H_5NH_3)Cl$.

On further cooling the crystal undergoes a second transformation at 181 K to the low temperature phase. The volume of the unit cell is doubled in relation to the initial one. The relatively sharp peak and the value of the thermal hysteresis for the low-temperature anomaly suggest that the observed phase transition is of first order related to the ordering process of the organic sublattice on lowering the temperature ($\Delta H_2 = 0.47$ kJ/mol and $\Delta S_2 = 2.12$ J/K mol). It suggests that the mechanism of the low temperature phase transition is connected with changes in motions of the cationic sublattice.

Crystal structures at 298 and 86 K

The structure was determined at 298 and 86 K, at r. t. and below the low-temperature first order phase transition detected at 181 K. At both temperatures, the crystals are triclinic, space group $P\bar{1}$. In the low-temperature phase the unit cell is approximately doubled along the diagonal direction between the *b* and *c*

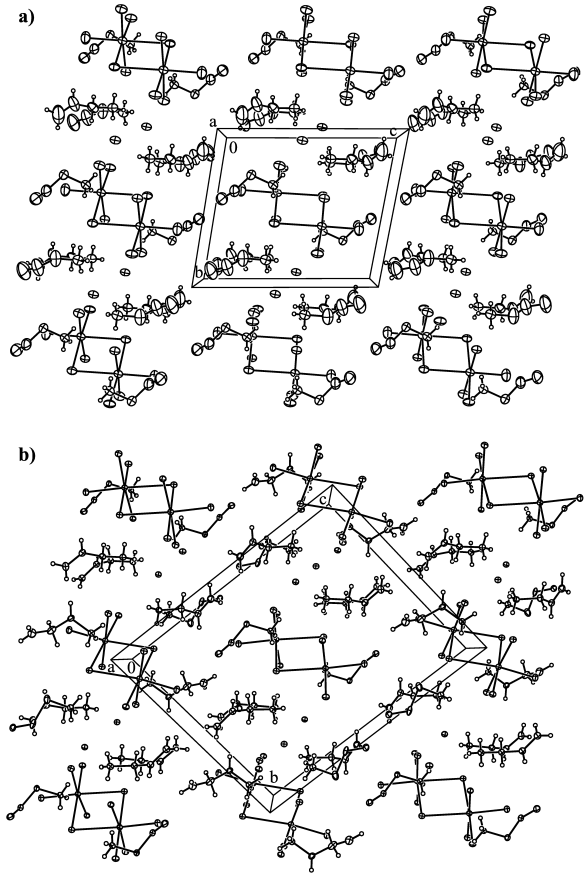

Fig. 2. The packing diagrams of $(C_3H_5NH_3)_2[SbCl_5]\cdot(C_3H_5NH_3)Cl$ at 298 (a) and 86 K (b). Displacement ellipsoids are plotted at the 25 % probability level. Only the more occupied carbon positions are shown for clarity.

axes compared to the unit cell of the room-temperature phase (Table 1, Fig. 2).

The room-temperature phase consists of three allylammonium cations (two are disordered), half of the $[Sb_2Cl_{10}]^{4-}$ unit and one isolated Cl^- anion. In the low-temperature phase, the crystal structure contains twice as many atoms – six allylammonium cations (two are disordered), two halves of the $[Sb_2Cl_{10}]^{4-}$ bioctahedral units and two isolated Cl^- anions. The setting of the cells and the labeling of atoms at 298 and 86 K (sets **A** and **B**) have been chosen to show the structural relationship between the positions of corresponding atoms in both phases (Fig. 2). The crystal data and the structure determination details at 298 and 86 K are listed in Table 1. The bond lengths and angles and the shortest N–H···Cl hydrogen bond geometries are presented in Tables 2 and 3, respectively.

Table 1. Crystal data and structure determination summary for $(C_3H_5NH_3)_2[SbCl_5]\cdot(C_3H_5NH_3)Cl$ at 298 and 86 K.

	298 K	86 K
Empirical formula	$C_9H_{24}N_3SbCl_6$	
Formula weight	508.76	
Color	colorless	
Crystal size [mm^3]	$0.2\times0.2\times0.1$	$0.3\times0.2\times0.2$
Crystal system	triclinic	
Space group	$P\bar{1}$	
Unit cell dimensions [Å, °]		
a	9.470(1)	9.437(1)
b	10.146(1)	13.523(1)
c	11.636(2)	16.542(1)
α	99.46(1)	84.38(1)
β	91.80(1)	84.38(1)
γ	102.59(1)	102.31(1)
Volume [Å^3]	1073.6(2)	2037.0(2)
Z	2	4
Density (calculated) [g · cm^{-3}]	1.574	1.659
Absorption coefficient [mm^{-1}]	2.024	2.134
Scan type	ω-scan	
Number of reflections used for cell determination	3795	4630
θ-range for data collection [°]	3.09 – 25.00	2.99 – 25.00
Index ranges	$-11\le h\le 11$	$-10\le h\le 11$
	$-7\le k\le 12$	$-16\le k\le 13$
	$-13\le l\le 13$	$-19\le l\le 19$
Reflections collected/unique	6695/3731	12496/7092
Refinement	Full-matrix least squares on F^2	
Data/parameters	3731/222	7092/366
Goodness of fit	1.000	1.061
Final R indices ($I\ge2\sigma(I)$)	$R_1 = 0.0385$	$R_1 = 0.0291$
	$wR_2 = 0.0942$	$wR_2 = 0.0694$
R indices (all data)	$R_1 = 0.0495$	$R_1 = 0.0348$
	$wR_2 = 0.1018$	$wR_2 = 0.0729$
Largest diff. peak and hole [e · Å^{-3}]	0.553 and −0.665	0.924 and −0.494

Structure at 298 K

The octahedral coordination of the Sb atoms within the $[Sb_2Cl_{10}]^{4-}$ unit, located at the inversion center, is far from regularity: the *cis* Sb–Cl–Sb angles vary from 83.55(4) to 102.34(3)°, whereas the *trans* angles are between 171.04(4) and 179.04(6)°. The longest Sb–Cl distances of 3.0647(15) and 3.1941(13) Å (Sb1–Cl1 and Sb1–Cl1^{I}, respectively) correspond to the bonds involving bridging chlorine atoms, while the shortest distances 2.3935(17) and 2.3976(12) Å (Sb1–Cl2 and Sb1–Cl5, respectively) belong to those involving terminal ligands, located opposite to the bridging ones. Two remaining Sb1–Cl3 and Sb1–Cl4 terminal bonds have intermediate bond lengths of 2.8254(12) and 2.4755(12) Å, respectively (Table 2).

Table 2. Selected bond lengths (Å) and angles (°) for $(C_3H_5NH_3)_2[SbCl_5] \cdot (C_3H_5NH_3)Cl$ at 298 and 86 K.

		86 K	
Atoms	298 K	A	B
Sb1–Cl1	3.0647(15)	3.0544(13)	3.1341(13)
Sb1–Cl1$^{I(II)(III)}$	3.1941(13)	3.2498(15)	3.1200(14)
Sb1–Cl2	2.3935(17)	2.4258(12)	2.3963(12)
Sb1–Cl3	2.8254(12)	2.7589(12)	2.7922(12)
Sb1–Cl4	2.4755(12)	2.5112(12)	2.5001(12)
Sb1–Cl5	2.3976(12)	2.3952(13)	2.4109(13)
Cl1–Sb1–Cl1$^{I(II)(III)}$	89.51(4)	90.34(4)	95.01(4)
Cl1–Sb1–Cl2	179.04(6)	176.59(3)	172.92(3)
Cl1–Sb1–Cl3	90.69(4)	87.85(3)	95.61(3)
Cl1–Sb1–Cl4	87.62(5)	89.98(3)	85.25(3)
Cl1–Sb1–Cl5	85.71(5)	87.86(4)	82.14(4)
Cl1$^{I(II)(III)}$–Sb1–Cl2	91.35(6)	88.66(4)	89.44(4)
Cl1$^{I(II)(III)}$–Sb1–Cl3	102.34(3)	104.26(3)	101.93(3)
Cl1$^{I(II)(III)}$–Sb1–Cl4	83.55(4)	84.34(4)	82.47(3)
Cl1$^{I(II)(III)}$–Sb1–Cl5	171.04(4)	171.50(3)	171.19(3)
Cl2–Sb1–Cl3	89.54(6)	89.24(4)	88.84(4)
Cl2–Sb1–Cl4	92.06(6)	93.16(4)	89.88(4)
Cl2–Sb1–Cl5	93.38(7)	93.60(4)	92.65(4)
Cl3–Sb1–Cl4	173.87(4)	171.13(3)	175.41(3)
Cl3–Sb1–Cl5	85.31(4)	83.97(4)	86.68(3)
Cl4–Sb1–Cl5	88.68(4)	87.35(4)	88.97(4)
Sb1–Cl1–Sb1$^{I(II)(III)}$	90.49(4)	89.66(4)	84.99(4)

Symmetry codes: ^{I} $-x+1, -y+1, -z+1$; ^{II} $-x+3, -y+3, -z+1$; ^{III} $-x+3, -y+2, -z$.

The same pattern of bond lengths order,

$$M\text{–}X_{(\text{bridging})} > M\text{–}X_{(\text{terminal}-\text{axial})} > M\text{–}X_{(\text{terminal}-\text{equatorial})},$$

was also found in other halogenoantimonate(III) and halogenobismuthate(III) salts composed of the isolated bioctahedral moieties, *e. g.* $[NH_3(CH_2)_2NH_3][BiCl_5] \cdot 2H_2O$ [18], $[4,4'\text{-}H_2bipy]_2[Bi_2Cl_{10}]$ [19], $(C_2H_5NH_3)_2[SbCl_5] \cdot (C_2H_5NH_3)Cl$ [20] and $(C_9H_7NH)_4[Bi_2Cl_{10}]$ [21].

Among all crystallographically non-equivalent allylammonium cations in the crystal structure of the title compound, one cation is ordered (N9), whereas the two remaining (N1 and N5) are disordered (Fig. 3). The occupancy factors for the split C atoms were refined until they converged, and then were fixed at 0.55 for C21, C31, C41, C71 and C81, and 0.45 for C22, C32, C42, C72, C82. Such a type of allylammonium cation disorder was also reported in our recent paper on the structure of $(C_3H_5NH_3)_3[BiCl_6]$ [13].

Without any interionic interactions, in the case of isolated $[SbCl_6]^{3-}$ octahedra, the Sb–Cl bonds in the entire environment of the Sb atom should have equal bond lengths and angles [22]. Taking into consideration the more complex bioctahedral moiety, the same values of bond lengths should be found for two bridging, two terminal bonds opposite to the bridging ones and two remaining terminal bonds. Since this is not the case, the distortions of the 5*s* electron lone pair (LEP) located on the Sb^{III} atom and the hydrogen bonds should be considered as the most important distorting factors [23, 24]. Indeed, the difference between the Sb1–Cl1 and Sb1–Cl1^{I} bond lengths (0.129(1) Å; Table 2) is undoubtedly caused by three hydrogen bonds involving the Cl1 atom, *i. e.* N1–H1C···Cl1, N5^{I}–H5B^{I}···Cl1 and N9–H9C···Cl1 (Fig. 4a, Table 3). The strongest influence on the enlargement of the Sb-Cl bond length arises from the N1–H1C···Cl1 hydrogen bond, which has the largest Sb1′—Cl1—H angle, close to 180° (172(1)°).

Table 3a. The strongest H-bonds (Å) and angles (°) for $(C_3H_5NH_3)_2[SbCl_5] \cdot (C_3H_5NH_3)Cl$ at 298 K.

D–H···A	D–H	H···A	D···A	D–H···A
N1–H1C···Cl1	0.90	2.44	3.302(4)	160
N5–H5B···Cl1^{I}	0.90	2.57	3.331(4)	143
N9–H9C···Cl1	0.90	2.39	3.262(4)	162
N5–H5C···Cl3^{III}	0.90	2.42	3.314(4)	170
N5–H5B···Cl4	0.90	2.76	3.331(4)	123
N1–H1A···Cl6^{I}	0.90	2.43	3.242(5)	150
N1–H1B···Cl6^{II}	0.90	2.38	3.266(4)	168
N5–H5A···Cl6	0.90	2.49	3.328(4)	155
N9–H9A···Cl6	0.90	2.42	3.292(4)	162
N9–H9B···Cl6^{II}	0.90	2.34	3.228(4)	168

Symmetry codes: ^{I} $x+1, y, z$; ^{II} $-x+1, -y+2, -z+1$; ^{III} $x-1, y, z$.

Table 3b. The strongest H-bonds and angles (°) for $(C_3H_5NH_3)_2[SbCl_5] \cdot (C_3H_5NH_3)Cl$ at 86 K.

D–H···A	D–H	H···A	D···A	D–H···A
N1A-H1C···Cl1A	0.90	2.34	3.238(3)	174
N5A-H5B···Cl1A^{I}	0.90	2.58	3.294(3)	137
N9A-H9B···Cl1A	0.90	2.39	3.249(3)	161
N5A-H5C···Cl3A^{II}	0.90	2.45	3.330(3)	166
N5A-H5B···Cl4A	0.90	2.74	3.338(3)	125
N1A-H1A···Cl6A^{III}	0.90	2.43	3.219(3)	147
N1A-H1B···Cl6B^{IV}	0.90	2.38	3.230(3)	158
N5A-H5A···Cl6A	0.90	2.50	3.334(3)	154
N9A-H9A···Cl6A	0.90	2.41	3.285(3)	163
N9A-H9C···Cl6B^{IV}	0.90	2.36	3.232(3)	162
N1B-H1E···Cl6A^{VI}	0.90	2.45	3.318(3)	161
N1B-H1D···Cl1B	0.90	2.37	3.199(3)	153
N5B-H5F···Cl1B^{V}	0.90	2.57	3.317(3)	141
N9B-H9F···Cl1B	0.90	2.42	3.251(3)	154
N5B-H5E···Cl3B^{III}	0.90	2.39	3.267(3)	164
N5B-H5F···Cl4B	0.90	2.70	3.301(3)	125
N1B-H1F···Cl6B^{II}	0.90	2.39	3.267(3)	165
N5B-H5D···Cl6B	0.90	2.54	3.339(3)	149
N9B-H9D···Cl6B	0.90	2.39	3.261(3)	164
N9B-H9E···Cl6A^{VI}	0.90	2.33	3.222(3)	173

Symmetry codes: ^{I} $-x+3, -y+3, -z+1$; ^{II} $x+1, y, z$; ^{III} $x-1, y, z$; ^{IV} $x, y, z+1$; ^{V} $-x+3, -y+2, -z$; ^{VI} $x, y, z-1$.

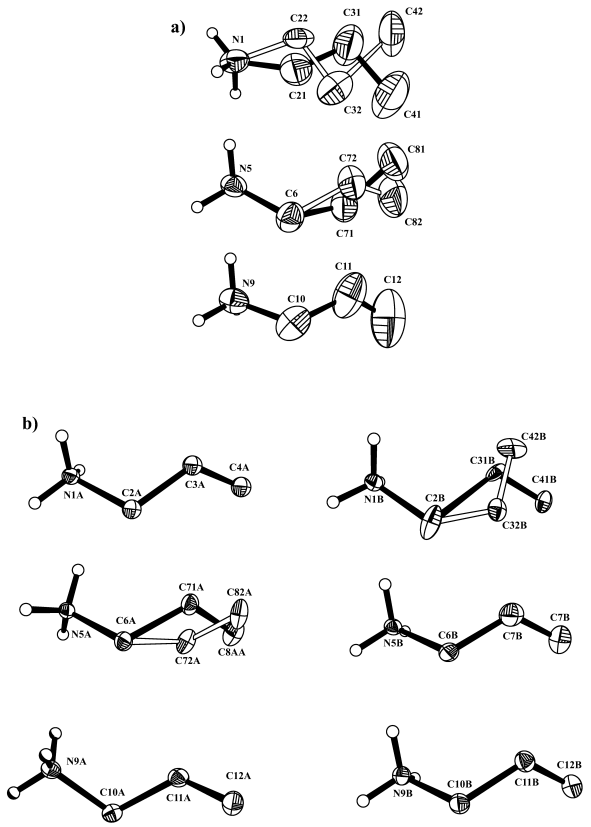

Fig. 3. The crystallographically independent allylammonium cations in the structure of $(C_3H_5NH_3)_2[SbCl_5] \cdot (C_3H_5NH_3)Cl$ at 298 (a) and 86 K (b). Displacement ellipsoids are at the 25 % probability level.

The $N5^{II}$–$H5C^{II}\cdots Cl3$ hydrogen bond causes an elongation of the Sb1–Cl3 (2.8254(12) Å) bond as well as an increase of the $Cl1^{I}$–Sb1–Cl3 angle (102.34(3)°). The elongation of the Sb1–Cl3 bond leads to the shortening of the Sb1–Cl4 bond located opposite (Table 2). A very similar pattern of interactions was also found in the structure of $(C_2H_5NH_3)_2[SbCl_5] \cdot (C_2H_5NH_3)Cl$ [20]. The difference between the longest and the shortest Sb-Cl bond length ($\Delta = 0.8006(17)$ Å) is caused mainly by the formation of the $[Sb_2Cl_{10}]^{4-}$ units, but also by the intermolecular N-H···Cl interactions.

Structure at 86 K

The arrangement of the chloro ligands around the two independent antimony(III) atoms at 86 K deviates more from the ideal octahedron [22] than in the room-temperature phase. The three different types of the Sb–Cl bond lengths are in the same order as in the structure determined at 298 K.

The "choosy" ordering process including N1 and N5 cations and simultaneously occurring conformational changes of N9 cation lead to a loss of part of the symmetry centers $(0, 1/2, 0; 0, 0, 1/2; 0, 1/2, 1/2; 1/2, 0, 1/2)$ on going from the room- to the low-temperature phase. The selective process of symmetry loss causes the formation of the new doubled unit cell with different diagonal *b* and *c* axes, whereas the *a* direction stays unchanged.

In the low-temperature phase relatively large changes on average for both symmetrically independent units in the corresponding Sb–Cl bond lengths and Cl–Sb–Cl angles are noted. The largest difference for the Sb-Cl bond lengths placed opposite is found at r. t. for the Sb1-Cl1′ and Sb1-Cl5 bonds. At 298 K ($\Delta = 0.7965(15)$ Å), this value is increased by 0.0581(15) Å ($\Delta = 0.8546(15)$ Å) in **A** and decreased by −0.0874(14) Å in **B** ($\Delta = 0.7091(14)$ Å) (see Fig. 4b, c). The r. t. bond lengths difference between Sb1-Cl1 and the opposite Sb1-Cl2 bond ($\Delta = 0.6712(17)$ Å) is different. It is decreased by 0.1426(17) Å in **A** ($\Delta = 0.5286(12)$ Å) and increased by 0.0666(13) Å in **B** ($\Delta = 0.7378(13)$ Å). The bond length changes are also observed for the Sb1-Cl4 and Sb1-Cl3 bonds. At r. t. the difference between the relevant lengths is 0.3499(12) Å. At low temperature the difference decreases by −0.1022(12) Å in **A** ($\Delta = 2477(12)$ Å) and −0.0578(13) Å in **B** ($\Delta = 0.2921(13)$ Å).

It should be noted, however, that on decreasing the temperature the distance between the Sb atoms inside the $[Sb_2Cl_{10}]^{4-}$ unit remains the same as at r. t. in **A** but it is significantly decreased (by 0.220(1) Å) in **B**. The distance between the Cl1 and Cl1′ atoms increases by 0.065(2) Å in **A** and by 0.203(2) Å in **B** while the Sb1-Cl1-Sb1 and Cl1-Sb1-Cl1 angles change much more in **B** (−5.50(4)°, 5.50(4)°) as compared to **A** (−0.83(4)°, 0.83(4)°). As at r. t., at 86 K a *trans*-influence is observed which consists of a shortening of the Sb-Cl bonds placed opposite to those which are elongated by bridging or N-H···Cl hydrogen bonding. The influence is mainly related to the stereochemical activity of the electron lone pair located on the Sb atom [23–25].

The main differences between the structures of the low- and room-temperature phases are associated with differences in the hydrogen-bonding patterns. The motions of the allylammonium cations decrease with low-

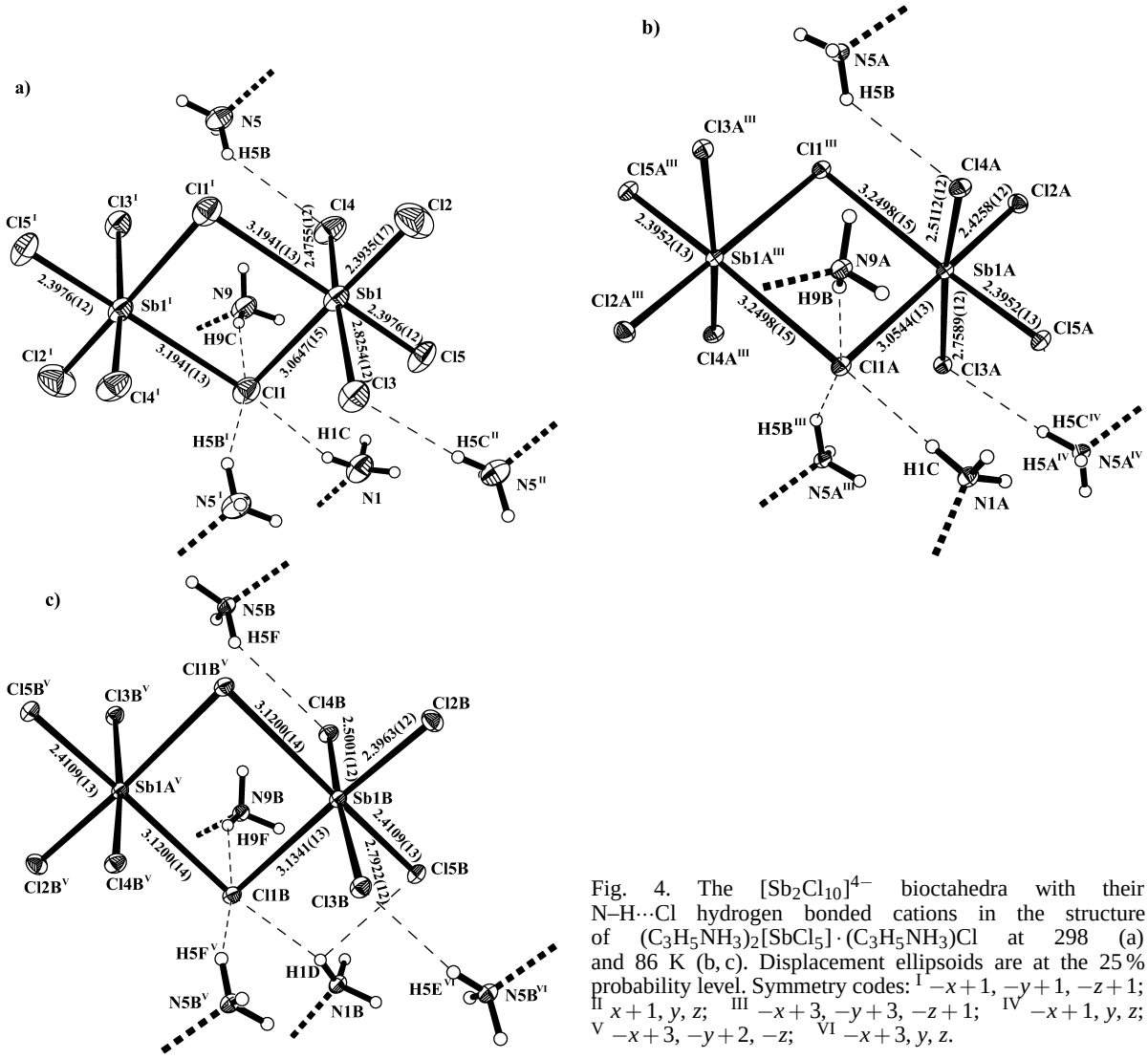

Fig. 4. The $[Sb_2Cl_{10}]^{4-}$ bioctahedra with their N–H···Cl hydrogen bonded cations in the structure of $(C_3H_5NH_3)_2[SbCl_5]\cdot(C_3H_5NH_3)Cl$ at 298 (a) and 86 K (b, c). Displacement ellipsoids are at the 25 % probability level. Symmetry codes: $^{I}\ -x+1, -y+1, -z+1$; $^{II}\ x+1, y, z$; $^{III}\ -x+3, -y+3, -z+1$; $^{IV}\ -x+1, y, z$; $^{V}\ -x+3, -y+2, -z$; $^{VI}\ -x+3, y, z$.

ering the temperature, and as a result in the low-temperature phase only two out of six symmetrically independent cations are disordered. The ordering processes of cations are associated with a decrease of the N···Cl distances. Taking into account that in both phases the types of anionic and cationic sublattices are the same, the differences described above are mainly related to the presence of the N–H···Cl interactions different in strength and geometry.

The largest difference of bond strength on lowering the temperature takes place for the N1-H1C···Cl1 hydrogen-bond. It is clearly seen looking at the changes in the hydrogen-bond geometry. The H1C···Cl1 distance and the N1-H1C···Cl1 angle at r. t. are equal to 2.44 Å and 160°, whereas at 86 K the largest changes are taking place in the cation **A** (Fig. 4b). The H···Cl distance decreases by 0.10 Å and the N-H···Cl bond angle increases to 174°, whereas for the cation **B** the decrease of the H···Cl distance is smaller (0.07 Å) and a decrease of the N-H···Cl angle to 153° is observed (Table 3b). The increase in strength of the N1A-H1C···Cl1A hydrogen bond leads to the enlargement of the Sb1′-Cl1 bond length from 3.1941(13) to 3.2498(15) Å ($\Delta = 0.0557(15)$ Å), and a small decrease of the bond length Sb1′-Cl5′ located opposite

($\Delta = -0.0024(13)$ Å). The situation in the anion **B** is different. There are two hydrogen bonds involving H1D, N1B-H1D···Cl1B and N1B-H1D···Cl5B. They lead to an enlargement of the Sb1-Cl5 bond length ($\Delta = 0.0133(13)$ Å) and a much smaller increase of the Sb1-Cl1′ bond length ($\Delta = 0.0059(14)$ Å). The strengthening of the two other hydrogen bonds involving the Cl1B atom has a stronger influence on its geometry, and as a result the Sb1-Cl1 bond length is increased from 3.0647(15) Å to 3.1341(13) Å ($\Delta = 0.0694(15)$ Å).

Conclusion

On cooling $(C_3H_5NH_3)_2[SbCl_5]\cdot(C_3H_5NH_3)Cl$ undergoes two phase transitions at $T_{c1} = 223$ K, of second order, and at $T_{c2} = 181$ K of first order. At r. t. and 86 K the space group is triclinic $P\bar{1}$.

Between T_{c1} and T_{c2} the structure is incommensurate with refined incommensurate q vectors of 0.072, −0.417, −0.454.

The crystal is composed of $[Sb_2Cl_{10}]^{4-}$ and Cl^- anions and allylammonium cations. At r. t. two out of three cations are disordered, whereas at 86 K the volume of the unit cell is doubled, and the number of disordered cations is lowered, two out of six being disordered.

The Sb-Cl bond lengths and Cl-Sb-Cl angles are mainly related to the structure of the anionic sublattice. A smaller influence on the geometry is exerted by the presence as well as the strength of the N-H···Cl hydrogen bonds.

The distorsions and geometry changes of the anionic sublattice on lowering the temperature are related to an increase in strength of the N-H···Cl hydrogen bonds.

Acknowledgements

Bartosz Zarychta is a holder of a scholarship (The Annual Stipend for Young Scientists) of The Foundation for Polish Science in 2006. We would also like to thank Dr. Michal Dusek for helpful discussions.

[1] A. Pietraszko, B. Bednarska-Bolek, R. Jakubas, P. Zieliński, *J. Phys.: Condens. Matter* **2001**, *13*, 6471.
[2] R. Jakubas, L. Sobczyk, *Phase Trans.* **1990**, *20*, 163.
[3] J. Zaleski, R. Jakubas, L. Sobczyk, J. Mróz, *Ferroelectrics* **1990**, *103*, 83.
[4] R. Jakubas, U. Krzewska, G. Bator, L. Sobczyk, *Ferroelectrics* **1988**, *77*, 129.
[5] H. Ishihara, K. Watanabe, A. Iwata, K. Yamada, Y. Kinoshita, T. Okuda, V. G. Krishnan, S. Dou, A. Weiss, *Z. Naturforsch.* **1992**, *47a*, 65.
[6] R. Blachnik, B. Jaschinski, H. Reuter, G. Kaster, *Z. Kristallogr.* **1997**, *212*, 874.
[7] R. Jakubas, *Structure and Phase Transitions in Alkylammonium Halogenoantimonates(III) and Bismuthates(III)*, Wrocław University Press, Wrocław, **1990**.
[8] J. Zaleski, *Structure, Phase Transitions and Molecular Motions in Chloroantimonates(III) and Bismuthates(III)*, Opole University Press, Opole, **1995**.
[9] L. Sobczyk, R. Jakubas, J. Zaleski, *Pol. J. Chem.* **1997**, *71*, 265.
[10] G. Bator, *Dielectric Relaxation and IR Studies on Phase Transitions in Alkylammonium Halogenoantimonates(III) and Bismuthates(III)*, Wrocław, **1999**.
[11] I. M. Vezzosi, L. P. Battaglia, A. B. Corradi, *Inorg. Chim. Acta* **1984**, *89*, 151.
[12] G. Bator, Th. Zeegers-Huyskens, R. Jakubas, J. Zaleski, *J. Mol. Struct.* **2001**, *570*, 61.
[13] B. Zarychta, M. Bujak, J. Zaleski, *Z. Naturforsch.* **2004**, *59b*, 1029.
[14] *Oxford Diffraction; CrysAlis CCD, Data collection GUI for CCD and CrysAlis RED, CCD data reduction GUI*, versions 1.171.24, Oxford Diffraction Poland, **2004**.
[15] G. M. Sheldrick, SHELXTL. Siemens Analytical X-ray Instrument Inc., Madison (Winsconsin, USA), **1990**.
[16] G. M. Sheldrick, SHELX-97, Program for the Solution and the Refinement of Crystal Structures, University of Göttingen (Germany), **1997**.
[17] V. Petříček, A. van der Lee, M. Evain, *Acta Crystallogr.* **1995**, *A51*, 529.
[18] S. Chaabouni, S. Kamoun, J. Jaud, *J. Chem. Cryst.* **1998**, *28*, 209.
[19] G. Alonzo, F. Benetollo, N. Bertazzi, G. Bombieri, *J. Chem. Cryst.* **1999**, *29*, 913.
[20] M. Bujak, J. Zaleski, *Pol. J. Chem.* **1999**, *73*, 773.
[21] F. Benetolo, G. Bombieri, A. Del Pra, G. Alonzo, N. Bertazzi, *Inorg. Chim. Acta* **2001**, *319*, 49.
[22] D. R. Schroeder, R. A. Jacobson, *Inorg. Chem.* **1973**, *12*, 210.
[23] X. Wang, F. Liebau, *Acta Crystallogr.* **1996**, *B52*, 7.
[24] J. Zaleski, A. Pietraszko, *Acta Crystallogr.* **1996**, *B52*, 287.
[25] R. J. Gillespie, *Chem. Soc. Rev.* **1992**, *21(1)*, 59.